Seasonal Evolution and Variability Associated with the West African Monsoon System

GUOJUN GU

Goddard Earth Sciences and Technology Center, University of Maryland, Baltimore County, Baltimore, and Laboratory for Atmospheres, NASA Goddard Space Flight Center, Greenbelt, Maryland

ROBERT F. ADLER

Laboratory for Atmospheres, NASA Goddard Space Flight Center, Greenbelt, Maryland

(Manuscript received 22 August 2003, in final form 5 March 2004)

ABSTRACT

In this study, the seasonal variations in surface rainfall and associated large-scale processes in the tropical eastern Atlantic and West African region are investigated. The 6-yr (1998–2003) high-quality Tropical Rainfall Measuring Mission (TRMM) rainfall, sea surface temperature (SST), water vapor, and cloud liquid water observations are applied along with the NCEP–NCAR reanalysis wind components and a 4-yr (2000–2003) Quick Scatterometer (Quik SCAT) satellite-observed surface wind product.

Major mean rainfall over West Africa tends to be concentrated in two regions and is observed in two different seasons, manifesting an abrupt shift of the mean rainfall zone during June–July: (i) near the Gulf of Guinea (about 5°N), intense convection and rainfall are seen during April–June and roughly follow the seasonality of SST in the tropical eastern Atlantic, and (ii) along the latitudes of about 10°N over the interior of the West African continent, a second intense rain belt begins to develop in July and remains there during the later summer season. This belt coexists with a northward-moving African easterly jet (AEJ) and its accompanying horizontal and vertical shear zones, the appearance and intensification of an upper-tropospheric tropical easterly jet (TEJ), and a strong low-level westerly flow. Westward-propagating wave signals [i.e., African easterly waves (AEWs)] dominate the synoptic-scale variability during July–September, in contrast to the evident eastward-propagating wave signals during May–June.

The abrupt shift of the mean rainfall zone thus turns out to be a combination of two different physical processes: (i) evident seasonal cycles in the tropical eastern Atlantic Ocean, which modulate convection and rainfall near the Gulf of Guinea by means of SST thermal forcing and SST-related meridional gradient; and (ii) the interaction among the AEJ, TEJ, low-level westerly flow, moist convection, and AEWs during July–September, which modulates rainfall variability in the interior of West Africa, primarily within the ITCZ rain band. Evident seasonality in synoptic-scale wave signals is shown to be a good indication of this seasonal evolution.

1. Introduction

A marked seasonal cycle exists in both the surface rainfall and large-scale environment over the West African region (e.g., Grist and Nicholson 2001; Le Barbe et al. 2002; Nicholson and Grist 2003). Major intense rainfall events appear near the Gulf of Guinea starting in April, move to the latitudes of about 10°N during the boreal summer, and then retreat back to the south after mid-September–October, manifesting the seasonal march of the ITCZ (e.g., Sultan and Janicot 2000; Le Barbe et al. 2002; Redelsperger et al. 2002). Time–latitude diagrams of monthly mean rainfall indicate that, suprisingly, this seasonal migration is characterized by an abrupt shift of the major rain zone during June–July (Sultan and Janicot 2000; Le Barbe et al. 2002; Redelsperger et al. 2002).

Sultan and Janicot (2000) first emphasized this phenomenon and showed that this shift may be associated with a westward-moving monsoon depression with a period of 20–40 days. This westward-propagating intraseasonal oscillation and its modulation of convection during the boreal summer were further documented in Sultan et al. (2003). Sultan and Janicot (2003) suggested that the interactions between the ITCZ convection, the westerly monsoon flow, the African easterly jet (AEJ), the heat-low dynamics, and the regional circulations due to the Atlas–Ahaggar Mountains are the major reasons for the abrupt shift of the ITCZ. The disappearance of the rainfall zone near the Gulf of Guinea was thus proposed to be caused by the intrusion of dry and subsiding air from the north, which is associated with the heat-low system. Redelsperger et al. (2002) also noticed this intraseasonal phenomenon accompanying the northward

Corresponding author address: Dr. Guojun Gu, NASA Goddard Space Flight Center, Code 912, Greenbelt, MD 20771.
E-mail: ggu@agnes.gsfc.nasa.gov

movement of the AEJ, even though the main purpose of their study was to describe multiscale convective activities within a synoptic-scale system. Le Barbe et al. (2002) detailed the annual cycle of rainfall in West Africa using a long record of surface gauge data from 1950 to 1990. They discovered the existence of (i) two rainy season regimes near the Gulf of Guinea during April–June and (ii) one single rainy season regime in the north around 10°N during the later summer season. It was suggested that two different dynamics may be in effect: one is associated with the continuous development of rain events near the Gulf of Guinea from February to May, and the other is an abrupt surge in mid-June with intense rainfall occurring synchronously between 9° and 13°N. Despite the nonlinear monsoon theory (Eltahir and Gong 1996) proposed to be a possible explanation for this phenomenon, no further details were pursued in their study. Lebel et al. (2003) categorized these two rainfall zones as ''oceanic'' and ''continental,'' suggesting their different physics. However, related processes behind this phenomenon, particularly the evolution of the oceanic zone, remain unclear and need to be quantified. This quantification will certainly enhance our understanding of certain fundamental mechanisms modulating rainfall variability over West Africa on both seasonal and interannual time scales.

A further detailed examination of surface rainfall on the weekly time scale shows that the abrupt shift or ''jump'' of major rain belts is actually a manifestation of the onset of intense convection and rainfall along 10°N and a simultaneous sudden termination of intense convection and rainfall along 10°N and a simultaneous sudden termination of intense convection and rainfall in the Gulf of Guinea (5°N) during the time period June–July (Fig. 4a). This seems to support the notion that two various processes are active near the latitudes of 5° and 10°N, respectively, and the peak rainfall seasons favored by these two processes are different due to different seasonal evolutions in the large-scale environment.

During the time period July–September, the large-scale atmospheric circulation features and changes, such as the AEJ, upper-tropospheric tropical easterly jet (TEJ), and monsoon related low-level moisture advection, etc., are commonly considered to be the major factors influencing rainfall variability in the mean rainband (e.g., Nicholson and Grist 2003). They thus possibly set the onset of surface rainfall along the latitude of 10°N within the interior of West Africa. Matthews (2004) recently documented a remote response to the Madden–Julian oscillation (MJO), suggesting a different intraseasonal variability pattern than Sultan et al. (2003). These two kinds of intraseasonal oscillations can both effectively modulate convection and rainfall over West Africa. High-frequency rainfall variability is significantly modulated by westward-propagating synoptic-scale waves [i.e., African easterly waves (AEW), e.g., Burpee 1972, 1974] and is also heavily contributed to by numerous intense mesoscale convective systems encouraged by the AEJ-related vertical shear (e.g., Rowell and Milford 1993; Laing and Fritsch 1993). Considering the peculiar rainfall transition pattern during June–July (Fig. 4a), it is interesting to examine whether a similar seasonal variation would exist in various dynamic features.

As an effective forcing mechanism for the tropical atmospheric circulation, global sea surface temperature (SST) patterns and time changes have been shown to play an essential role in rainfall variability over West Africa on the interannual and interdecadal time scales (e.g., Lamb and Peppler 1992; Fontaine and Janicot 1996; Janicot et al. 1998), particularly the SST anomalies in the tropical eastern Pacific (mostly associated with the ENSO events), and the tropical eastern and northeastern Atlantic. On the seasonal time scale, the evident seasonal cycle in the tropical eastern Atlantic thus may naturally be a direct forcing mechanism on rainfall variability at least in the Gulf of Guinea. Opoku-Ankomah and Cordery (1994) showed that a strong positive correlation exists between the SST in the tropical eastern Atlantic and rainfall variability in Ghana just north of the coastline in the Gulf of Guinea. Grodsky and Carton (2001) even reported a near-equatorial, coupled intraseasonal oscillation in this region. In this study, therefore, we will argue that seasonal variations in the surface rainfall near the Gulf of Guinea, where the rainfall peaks during May–June, are primarily modulated by the seasonal forcing from the ocean. In contrast, the rainfall and variability within the interior of West Africa primarily result from the interactions among various dynamic components partly shown in previous studies (e.g., Nicholson and Grist 2003).

The paper is organized as follows: Section 2 describes the datasets used in this study. Seasonal variations in the tropical eastern Atlantic and West Africa are presented in section 3, which includes detailed descriptions of the evolution of the cold-tongue complex on the monthly and weekly time scales by means of the recently available satellite observations, and the seasonal cycle in mean zonal wind field over the tropical eastern Atlantic and West African sector. Synoptic-scale rainfall variability is also investigated in section 3 by applying a 2D wavelet spectrum analysis (Gu and Zhang 2001). In section 4, the main results are summarized and discussed.

2. Data

Two 6-yr (1998–2003) Tropical Rainfall Measuring Mission (TRMM) products [3B43 (monthly) and 3B42 (daily)] are applied to quantify the seasonal variation of rainfall patterns and associated synoptic-scale perturbations within the West African monsoon region. These two TRMM datasets are produced by using the (nearly) coincident TRMM Combined Instrument [TCI, the combined TRMM Microwave Imager (TMI) and Precipitation Radar (PR) algorithms] and TRMM Visible and

Infrared (IR) Scanner (VIRS) data to calibrate geosynchronous IR rain rates (Adler et al. 2000), providing much better rain-rate estimates than those solely derived from the geo–IR observations, but with the same superior time sampling. Both datasets are on a 1° × 1° grid, cover a global belt approximately from 40°S to 40°N and extend from 1 January 1998 to 31 December 2003. These TRMM products have been validated against rain gauge and ground-based radar data over the Tropics on a monthly scale (Adler et al. 2000, 2003) with the daily product showing a moderate positive bias, from 12% to 30%, depending on the period used and the type of comparison data. Nicholson et al. (2003) specifically validated these and other TRMM products over West Africa, finding a very small overall bias (+4%) for the daily product during May–September, although the June bias peaked at +20% in the year examined (1998). The TRMM merged monthly product incorporates gauge information on a monthly basis into the analysis so that its bias is zero in the Nicholson et al. (2003) analysis. Correlations between the satellite products and the gauges on a monthly scale are also shown to be very good (approximately 0.9). In this study, we will concentrate on the rainfall variability within the region of about 9.5°W–9.5°E over West Africa and the tropical eastern Atlantic to limit the effects of the western coast and central Africa.

The SST data are retrieved from the TMI on board the TRMM satellite. With a distinct advantage over the traditional IR estimates that require a cloud-free field of view, TMI provides a continuous coverage of tropical SST (Wentz et al. 2000). The data covers a global region extending from 40°S to 40°N at a spatial resolution of 0.25°. Monthly and weekly TMI SST products are applied in this study, together with the columnar water vapor (VW) and cloud liquid water (LW) data retrieved also from the TMI (detailed algorithms are described in Wentz 1997). The spatial patterns and seasonal variations in TMI SST in the tropical Atlantic are further compared to those described by the Reynolds and Smith (1994) SST data, which covers 89.5°S–89.5°N and are on a 1° grid.

Surface wind fields are obtained from the SeaWinds scatterometer on board the Quick Scatterometer (QuikSCAT) satellite (Liu et al. 1998; Liu 2002). Monthly and weekly products from 2000 to 2003 are applied, extending from 89.875°S–89.875°N and with a spatial resolution of 0.25°.

Monthly zonal wind components from the National Centers for Environmental Prediction–National Center for Atmospheric Research (NCEP–NCAR) reanalysis project (Kalnay et al. 1996) are used to provide a description of large-scale circulation patterns over the tropical Atlantic and West African region. Archived on a 2.5° × 2.5° grid, only data from 1998 to 2003 are applied corresponding to the current record length of the TRMM 3B43 and 3B42.

3. Results

Spatial distributions of monthly mean rainfall, SST, and surface wind vectors over the Atlantic–African sector are shown in Fig. 1. The oceanic ITCZ, represented by a rainfall band, moves northward and gradually intensifies during boreal spring–summer. It reaches its northernmost position and becomes strongest in August, then retreats back to the south and weakens thereafter. This oceanic ITCZ is generally collocated with warmer SST (>27°C) and the surface confluence line. Particularly with the formation and intensification of a cold tongue in the tropical eastern Atlantic during June–August, the major rainfall zone in the Gulf of Guinea seems to move along the coastline to the western coast not directly northward, roughly following the movement of the warmer SST zone (>27°C), suggesting the modulation of rainfall by both the land surface and SST-related processes. The land surface conditions north of the coastline in the Gulf of Guinea may not be favorable for the development of rainfall events during this time period. This is quite different from the situations in the eastern Pacific where the ITCZ-related mean rainfall band moves continuously to the north during boreal spring–summer.

Within the West African continent, intense rainfall appears in April right across the coastline in the Gulf of Guinea (Fig. 1). The mean rainfall band becomes strong in June but still remains in the coastal region (5°N). In August, the most intense rainfall band has already moved to the latitudes of about 10°N. Land rainfall retreats back to the south and becomes weaker during boreal fall–winter. Major rainfall events in the Gulf of Guinea are observed mostly over the ocean in December (Fig. 1), corresponding to the return of relatively warmer SST in the Gulf of Guinea due to surface wind relaxation (e.g., Weingartner and Weisberg 1991). Between June and August, the major rainfall band does not show a continuous march to the north, but instead two rainfall zones seem to appear independently at two different latitudinal belts (5° and 10°N) (Fig. 4a). As proposed in section 1, these two rainfall zones may be modulated by two different physical processes. Detailed seasonal variations in several variables are thus investigated in the following two sections to explore the related physical processes. A 2D wavelet spectrum analysis is further applied to examine the various components in these two rainfall zones.

a. Cold tongue complex

1) MONTHLY MEAN

Figure 1 provides a basic pattern of seasonal evolution in SST in the tropical Atlantic. In the Gulf of Guinea, SST reaches its maximum in April and minimum in August, showing the life cycle of the cold tongue complex. Detailed monthly changes are given in Fig. 2 for the time period February–August, the most intense rain-

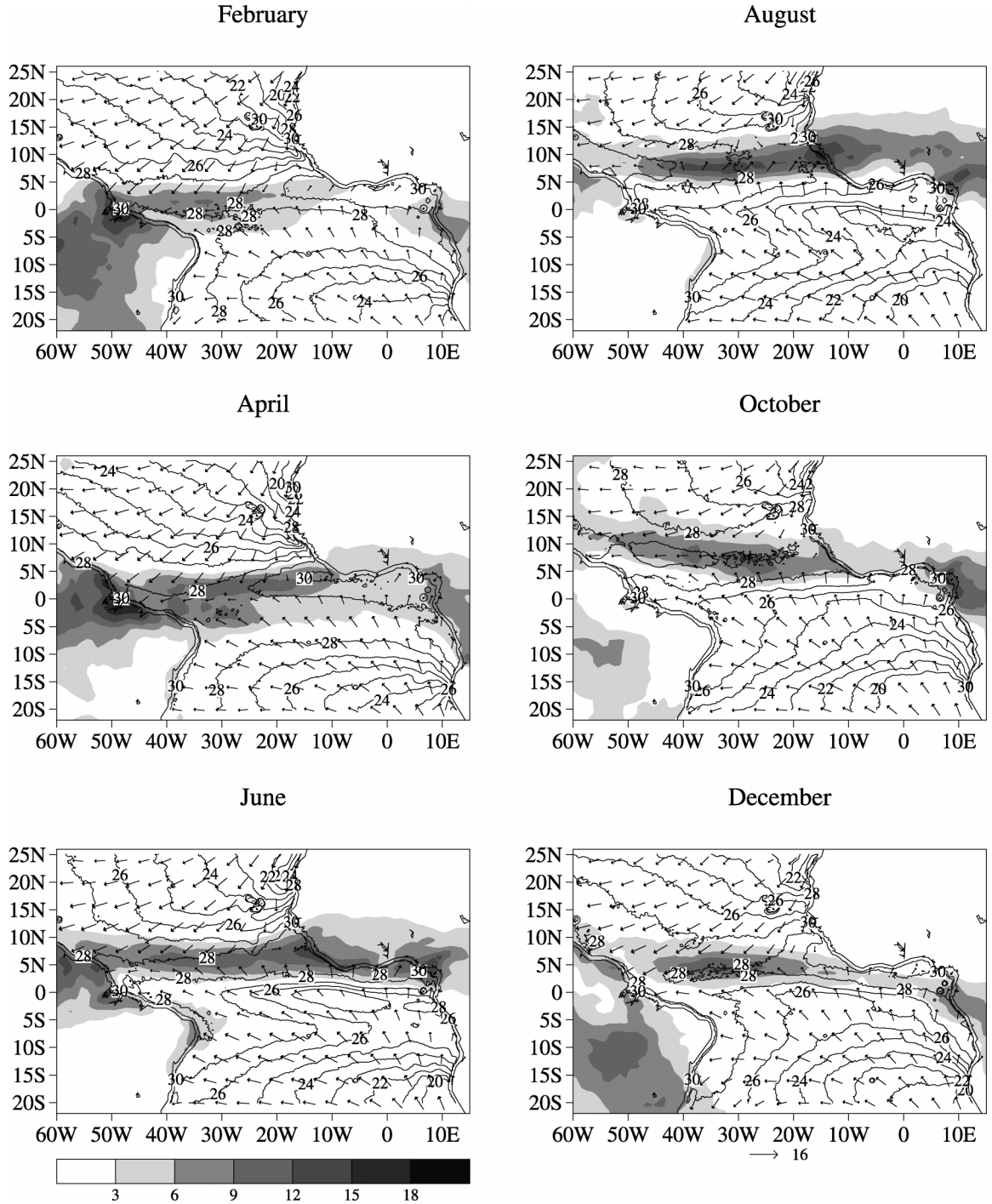

FIG. 1. Monthly mean rainfall (mm day^{-1}) from 3B43 (shaded), TMI SST (°C; contours), and QuikSCAT wind vectors (m s^{-1}; only from 2000 to 2003) in the Atlantic–West African sector. Wind vectors of magnitudes <0.5 m s^{-1} are not plotted.

fall transition season. During February–April, surface rainfall increases along the oceanic ITCZ and in the Gulf of Guinea. Surface wind changes a little, and only a weak northerly acceleration can be seen in the middle of the tropical Atlantic. SST increases in most of the tropical Atlantic except the regions right off the western coast and north of 15°N. From April to June, significant rainfall increases are seen between 5°–15°N, with sharp decreases south of about 5°N. Simultaneously, an evident acceleration of southerly wind appears. SST drops south of about 5°N, especially in the Gulf of Guinea, indicating the oncoming cold phase. SST increases north

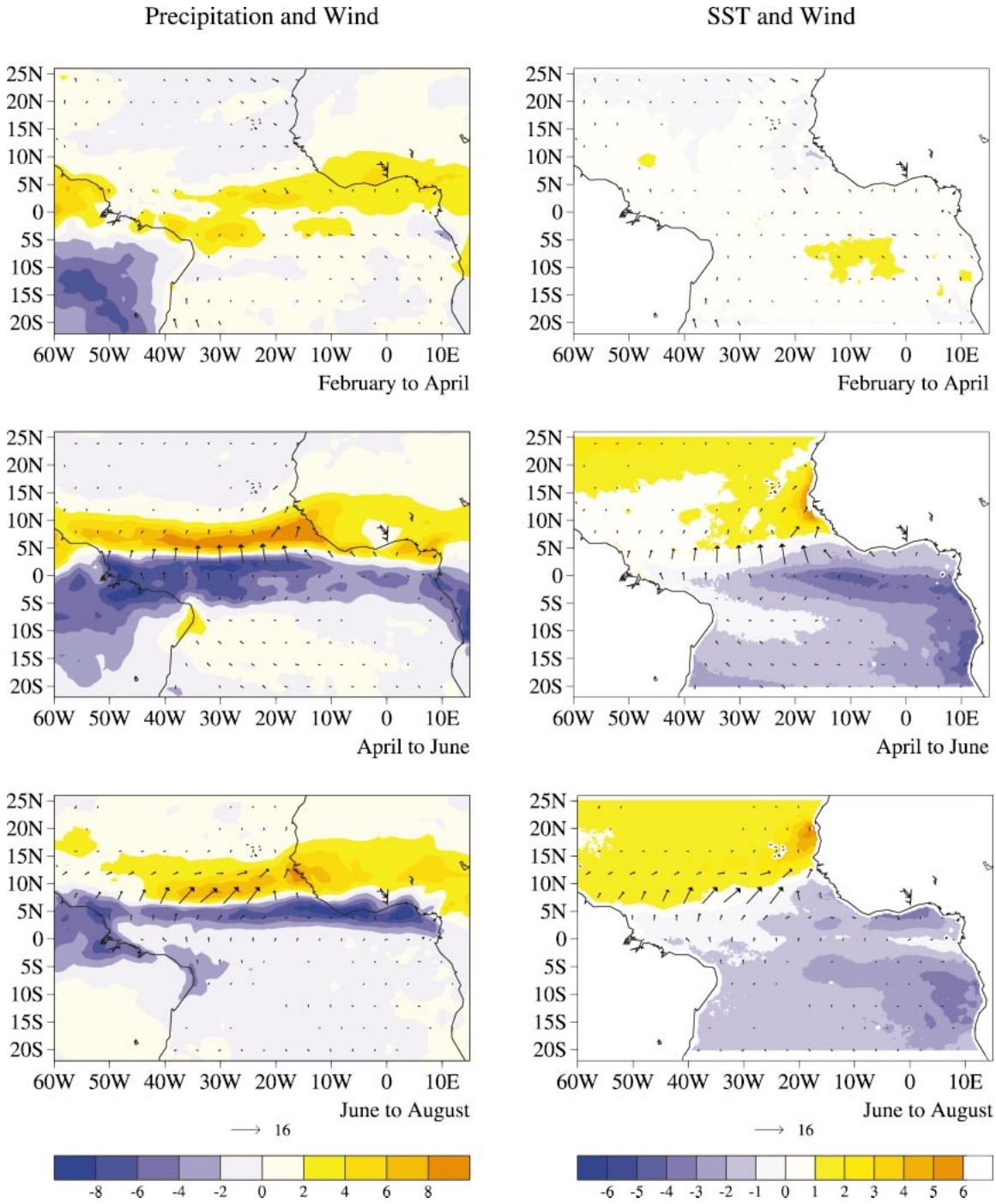

FIG. 2. Monthly changes in mean rainfall (mm day^{-1}) from 3B43, TMI SST (°C), and QuikSCAT wind vectors (m s^{-1}; only from 2000 to 2003) in the Atlantic–African sector. Wind change vectors of magnitudes <0.5 m s^{-1} are not plotted.

of 5°N, mostly off the western coast and north of 15°N. It is interesting to note that an observable minimum in rainfall increase occurs between 5° and 10°N at 0°, north of the coastline in the Gulf of Guinea, possibly due to the occurence of coastal upwelling. This land area is known as the ''Togo-gap.''[1] During June–August, the positive rainfall change zone moves farther to the north,

[1] One reviewer specifically mentioned this climatological phenomenon and its possible physical mechanism.

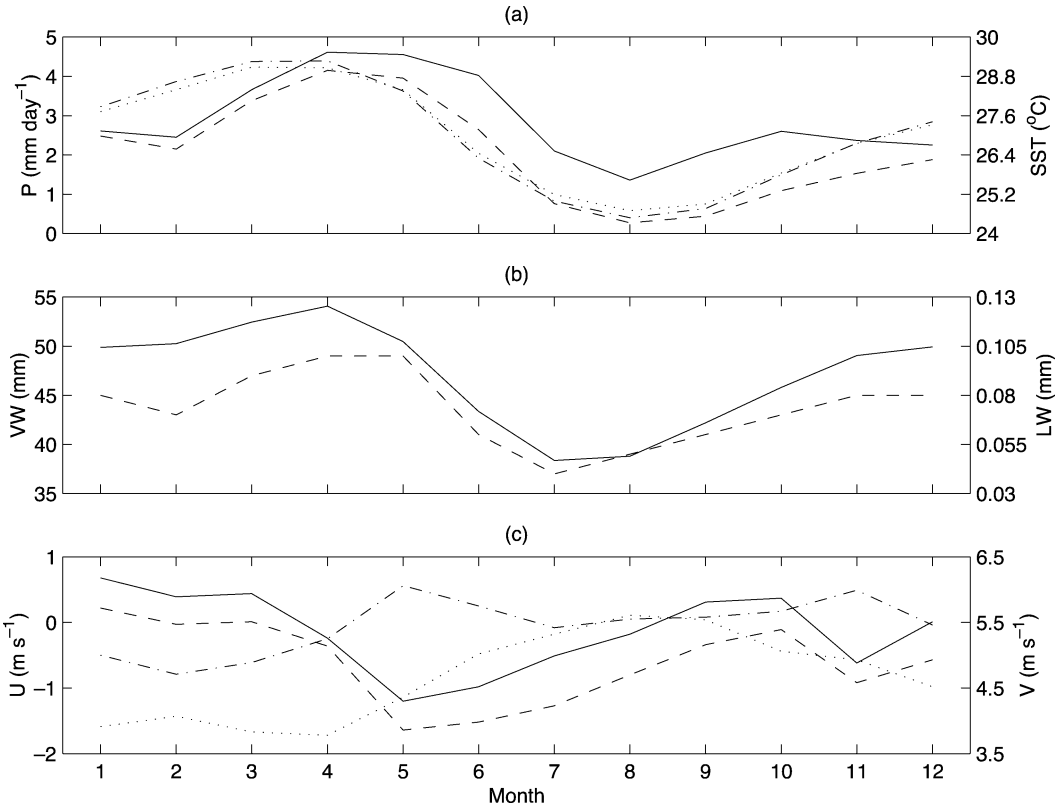

FIG. 3. Seasonal cycles in (a) rainfall [P (mm day^{-1})] from 3B43 [4.5°S–6.5°N, 9.5°W–9.5°E (solid line) and 4.5°S–4.5°N, 9.5°W–5.5°E (dashed line)], TMI SST (°C; 4.125°S–4.125°N, 10.125°W–5.125°E; dashed–dotted line), and Reynolds and Smith (1994) SST (°C; 4.5°S–4.5°N, 9.5°W–4.5°E; dotted line); (b) TMI VW (mm; solid line) and LW (mm; dashed line; 4.125°S–4.125°N, 10.125°W–5.125°E; and (c) QuikSCAT zonal [U (m s^{-1}); solid line] and meridional winds [V (m s^{-1}); dashed–dotted line; 4.125°S–4.125°N, 10.125°W–5.125°E], and NCEP–NCAR 1000-mb zonal [U (m s^{-1}); dashed line] and meridional winds [V (m s^{-1}); dotted line; 5°S–5°N, 10°W–5°E]. (c) is only from 2000 to 2003.

concurrently with the positive SST change and southwesterly wind increase. In the Gulf of Guinea, strong negative rainfall changes indicate the termination of major rainfall events, concomitant with the continued SST drop (<27°C). This evolution pattern is basically in agreement with Mitchell and Wallace (1992).

We further narrow our concentration on the domain–mean seasonal cycles in the Gulf of Guinea and the land just north of it between 10°W and 10°E (Fig. 3). For SST, VW, LW, and surface wind components, the domain is right across the equator in the eastern Atlantic and approximately covers 4.5°S–4.5°N and 10°W–5°E. Two domains are used to represent rainfall variability: (i) 4.5°S–6.5°N, 9.5°W–9.5°E and (ii) 4.5°S–4.5°N, 9.5°W–5.5°E. Annual cycles in rainfall are very similar within these two domains except that a weak semiannual cycle is seen in the first domain (Fig. 3a), a manifestation of the seasonal march of the ITCZ over land. The warmest SST is observed during March–April, with the coldest SST during July–September. We would also note that no significant difference is found between TMI SST and Reynolds and Smith (1994) SST (dashed–dotted and dotted lines, respectively, in Fig. 3a) except that more details can be seen in the spatial patterns in TMI SST (not shown).

Surface rainfall, VW, and LW generally follow the seasonal cycle in SST (Figs. 3a,b), showing the importance of oceanic surface thermal forcing. Previous studies have examined this forcing (e.g., Zhang 1993; Lau et al. 1997). Higher SST tends to induce at least qualitatively more rainfall (e.g., Neelin and Held 1987). However, the peak season in rainfall arrives during April–May and is about a month later than for SST (Fig. 3a). This 1-month lag possibly leaves space for other factors to play a role, such as the large-scale circulation (e.g., Lau et al. 1997). Maloney and Kiehl (2002) showed a similar time lag of about 10 days between the highest SSTs and maximum convection in the tropical eastern Pacific, which occurs during a composite life cycle of the MJO.

Strong surface wind changes during the March–June season are observed by the QuikSCAT satellite; zonal wind quickly changes from westerly to easterly (solid line in Fig. 3c), along with a sharp increase of southerly meridional wind (dashed–dotted line in Fig. 3c). These wind changes seem to be a direct response to the con-

TABLE 1. Correlation coefficients (γ) between weekly rainfall [P (mm day^{-1}); 4.5°S–6.5°N, 9.5°W–9.5°E], TMI SST [°C; 4.125°S–4.125°N, 10.125°W–5.125°E], VW (mm; 4.125°S–4.125°N, 10.125°W–5.125°E), and LW (mm; 4.125°S–4.125°N, 10.125°W–5.125°E) during 1998–2003. Here, $\gamma = 0.354$ is the 1% confidence level based on 50 dof.

γ	1998	1999	2000	2001	2002	2003
P and SST	0.45	0.58	0.53	0.67	0.55	0.5
P and VW	0.59	0.6	0.64	0.62	0.53	0.62
P and LW	0.69	0.81	0.67	0.76	0.74	0.73
VW and SST	0.89	0.86	0.83	0.87	0.87	0.83
LW and SST	0.61	0.66	0.49	0.57	0.52	0.53
LW and VW	0.79	0.78	0.7	0.67	0.67	0.77

vection and rainfall near the coastline (e.g., Mitchell and Wallace 1992; Li and Philander 1997). Due to the shallowness of the thermocline in this part of the ocean, SST is very sensitive to the varying surface wind field (e.g., Merle 1980; Weingartner and Weisberg 1991). The equatorial upwelling process is thus immediately enhanced and SST drops, which eventually forms a cold tongue complex (e.g., Mitchell and Wallace 1992; Li and Philander 1997). With continued SST drop, rainfall reaches its lowest amount during July–September, concurrent with the decrease of VW and LW, further showing the impact of SST on convection and rainfall. Hence, surface rainfall in this region actually plays two roles: passively following the seasonal variations in SST, and actively participating in the formation of the equatorial cold tongue and the completion of the annual cycle in the entire air–sea coupled system.

2) WEEKLY MEAN

Weekly products from the TRMM satellite are assessed to further examine seasonal cycles in various variables and their relationships in the Gulf of Guinea. The SST forcing is evident. Higher (lower) SST generally corresponds to more (less) VW, LW, and surface rainfall (not shown). Strong linear relations are also seen among VW, LW, and rainfall. Thus, it is not surprising that their linear correlation coefficients are all above the 1% confidence level based on 50 degrees of freedom (dof; 52 weeks yr^{-1}; Table 1).

The seasonal variations in rainfall and SST are illustrated in Figs. 4a and 4b, respectively. Consistent with the monthly results, intense rainfall is observed at two different seasons and two different regions (Fig. 4a). A sharp reduction of rainfall south of 5°N occurs at days 190–200 (i.e., mid-July), resulting from cold SST damping. Warmer SST generally corresponds to rainfall events south of 5°N within the Gulf of Guinea before day 190. However, a lag phase is evident between the maximum rainfall and warmest SST as shown in Fig. 3. It is further noted that the most intense rainfall zone in the region actually comes with the appearance of strong meridional SST gradients (Fig. 4c), despite the fact that the mean SST has to be above a certain threshold (at least 26°C; Fig. 4b). This suggests the importance of both direct SST forcing and its related dynamic (gradient) forcing in organizing surface convergence, convection, and rainfall, a result that is generally consistent with previous studies (e.g., Neelin and Held 1987; Lindzen and Nigam 1987).

Weekly surface wind components averaged in the tropical eastern Atlantic are shown in Fig. 5. As in Fig. 3c, the surface wind changes direction from southwesterly to southeasterly around day 120. Particularly, an abrupt increase in the meridional wind component occurs during days 120–150, confirming the monthly results. Despite high-frequency variabilities in surface wind components on the weekly time scale, coherent relations between zonal and meridional winds are discernible, which is especially clear in Fig. 5c. Within this region, surface trade wind direction always shifts from southwesterly to southeasterly or vice versa.

b. Mean zonal wind field

Previous studies indicate that summer rainfall variability over West Africa is closely associated with the variabilities in the large-scale environment on both interannual and seasonal time scales (e.g., Grist and Nicholson 2001; Nicholson and Grist 2003). Mesoscale rainfall systems and AEWs are also closely associated with the large-scale dynamic features, such as the AEJ, TEJ, and low-level flow (e.g., Rowell and Milford 1993; Burpee 1972, 1974). To provide a full seasonal pattern of rainfall over the tropical eastern Atlantic–West Africa region and its related large-scale processes, we further emphasize these large-scale atmospheric features using the zonal wind component from the NCEP–NCAR reanalysis project (see comparisons with the QuikSCAT surface winds in the appendix).

As in Fig. 4a, surface rainfall shows a significant break during days 180–200 (or June–July; Fig. 6). There is an abrupt development in the low-level westerly flow, quantified by the zonal wind at 850 mb, which is concomitant with the onset of the rain events along 10°N. The same peak season (July–September) for this low-level westerly flow and surface rainfall in the interior of West Africa strongly suggests their internal connection, since the moisture transport from the Gulf of Guinea during this season could have been heavily reduced due to the development of the oceanic cold tongue (Figs. 1, 3, and 4).

The AEJ moves northward and becomes stronger in the spring (Fig. 6c). It achieves its maximum intensity during April–June. In June, the center of the AEJ is already near 10°N. It becomes weaker during days 180–200 (July), possibly related to the appearance of the intense AEWs, which tend to weaken the AEJ (Fig. 7). The AEJ strengthens a little during August–September before it becomes weaker again and moves back to the south during the boreal fall and winter.

The TEJ is another important summer feature over

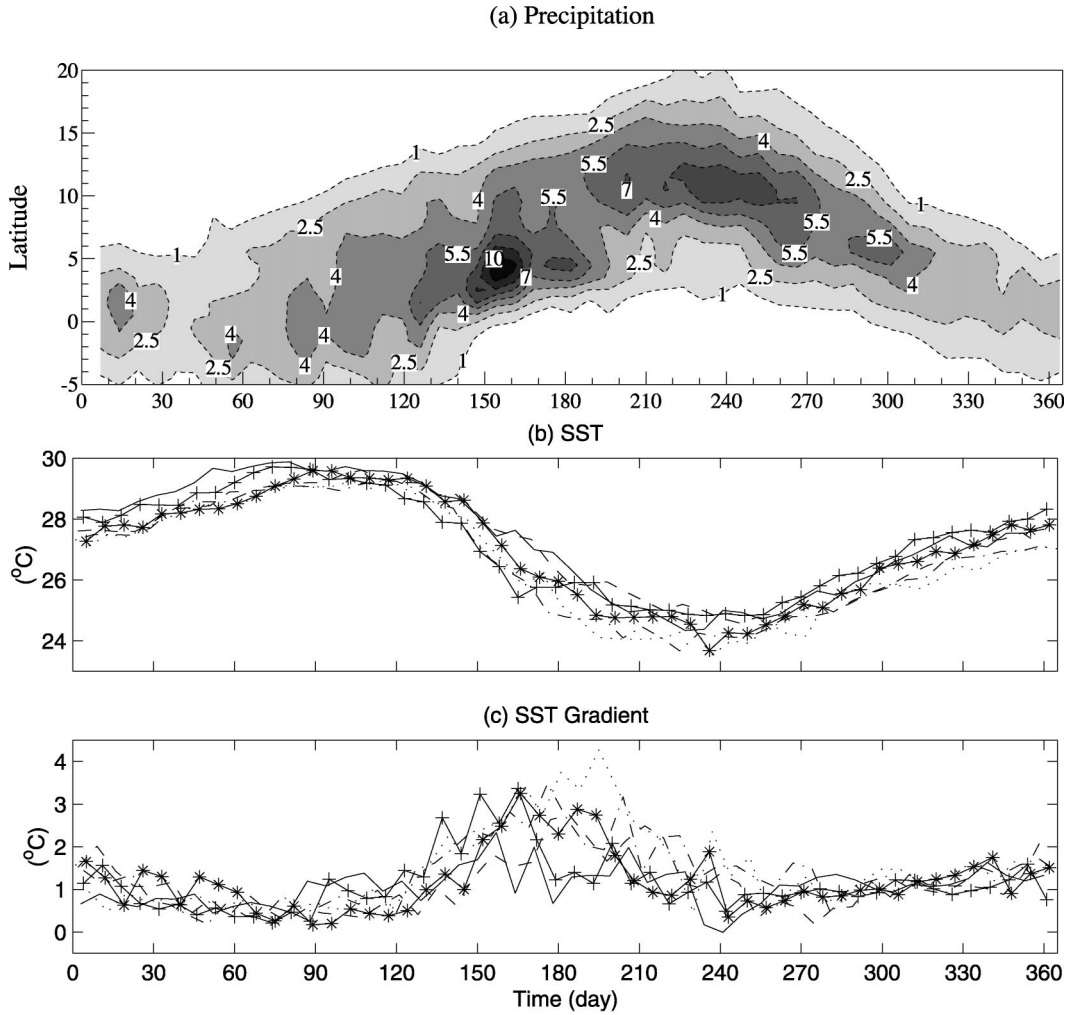

FIG. 4. Seasonal cycles in (a) weekly rainfall (mm day^{-1}) between 9.5°W and 9.5°E, (b) weekly TMI SST (°C; 4.125°S–4.125°S–4.125°N, 10.125°W–5.125°E), and (c) weekly TMI SST differences between 2.125°N and 0.125°S, averaged along 10.125°W–5.125°E. In (b) and (c), solid lines are used for 1998, dashed lines for 1999, dashed–dotted lines for 2000, dotted lines for 2001, lines with asterisks (*) for 2002, and lines with crosses (+) for 2003.

West Africa because of its associated large-scale upper-level divergent motion. As with the low-level westerly flow, a sudden development of the TEJ is also observed approximately at the same time period, that is, around day 180. This jet is generally considered to be related to the summer Indian monsoon processes (e.g., Hastenrath 1991), even though it could exist year-round and move to the Southern Hemisphere during the boreal winter (Nicholson and Grist 2003). These concurrent transition features in these various fields explicitly suggest the dynamic control of convection and rainfall over West Africa during the boreal summer (e.g., Grist and Nicholson 2001).

c. *Rainfall-related perturbations*

In this section, the surface daily rainfall patterns over the tropical eastern Atlantic and West Africa are further decomposed into various perturbation signals, particularly within the synoptic-scale domain (here referred to as wavenumber $k = 6$ to 10). The effort is to explore whether any season-and/or latitude-dependent wave modes exist in surface rainfall variability, taking into account the evident seasonal transition of rainfall (Figs. 4a and 6a). A 2D wavelet spectrum analysis is applied to extract the regional spectral power of perturbations within the wavenumber–frequency domain (Gu and Zhang 2001). As in Gu and Zhang (2001), a 92-day running window is applied to estimate the monthly mean spectral power within these 6 yr.

Figure 7 illustrates the latitude–frequency diagrams of the mean spectral power with $k = 6$ to 10 during April–June and July–September. Evident seasonal variations are seen in both the strength of spectral signals and their preferred frequency ranges. Most of the spectral signals move to the north, following the seasonal

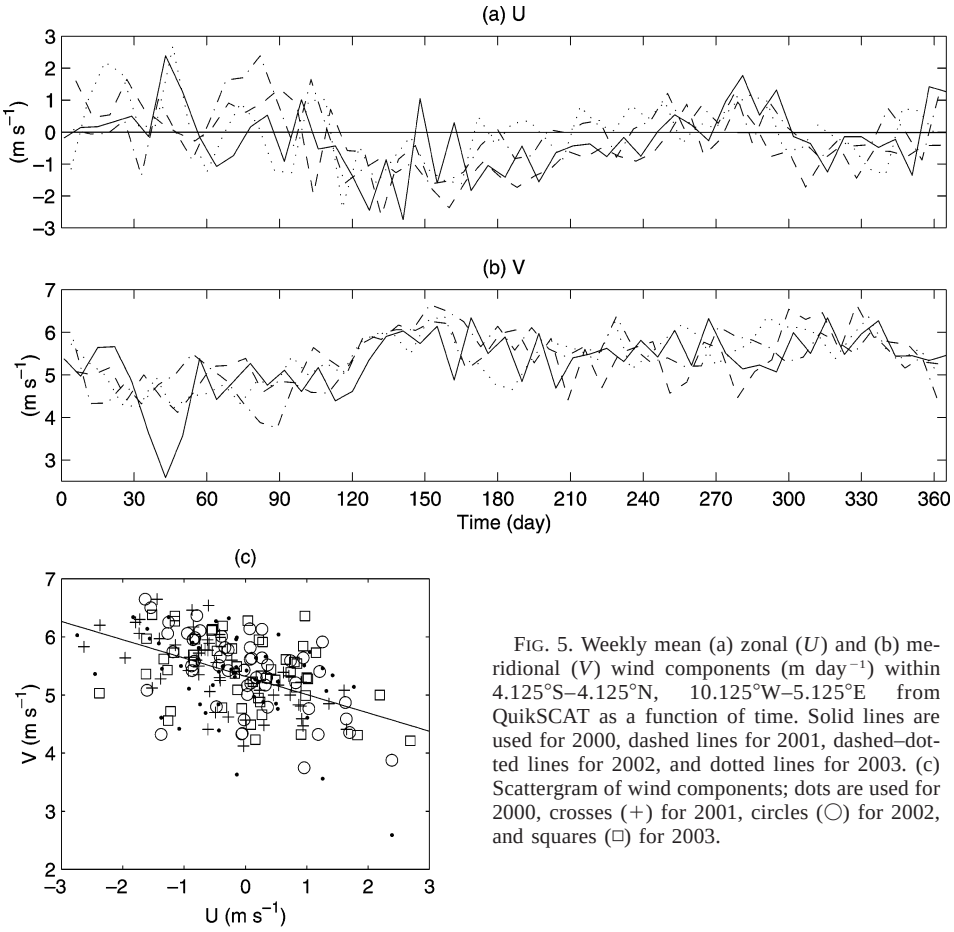

FIG. 5. Weekly mean (a) zonal (U) and (b) meridional (V) wind components (m day^{-1}) within 4.125°S–4.125°N, 10.125°W–5.125°E from QuikSCAT as a function of time. Solid lines are used for 2000, dashed lines for 2001, dashed–dotted lines for 2002, and dotted lines for 2003. (c) Scattergram of wind components; dots are used for 2000, crosses (+) for 2001, circles (○) for 2002, and squares (□) for 2003.

migration of major rain events. During April–June, the perturbation signals are weak and tend to be close to the equator. Propagating signals with frequencies $f > 0$, that is, eastward propagating, dominate and are concentrated along 2°–6°N. Two major eastward-propagating power peaks are located roughly at $f = 0.1$ and $f = 0.2$ cycles per day (cpd), respectively. Thus, within the synoptic-scale domain, the rain events at the latitudes of 5°N shown in Figs. 4a and 6a are primarily composed of eastward-propagating perturbations that may be associated with the Kelvin-type tropical waves forced by warm SST (e.g., Wheeler and Kiladis 1999). In contrast, during July–September, westward-propagating signals are dominant within a frequency band of -0.1 to -0.3 cpd, corresponding to the intense AEW activity and major rain events along 10°N (Figs. 4a and 6a).

The mean spectral power for those smaller-wavenumber perturbations ($k = 1$ to 5) is shown in Fig. 8. An evident power peak is seen at a frequency range of $f = 0.02$ to 0.04 cpd. Contrasting to their synoptic-scale counterparts, these wave signals are always eastward propagating, though their is a seasonal migration in their preferred latitudes roughly following the seasonal march in surface rainfall. We suggest that these wave signals might be related to the classic tropical intraseasonal variability, that is, the MJO, which is already identified in a recent study (Matthews 2004), though local convection–circulation interactions can generate the MJO-type oscillation as well. Since the MJO-related convective signals are considered to be primarily confined to the Indian and western Pacific Oceans (i.e., Hendon and Salby 1994) and not much work has been done in the Atlantic–West African sector, detailed mechanisms behind these rainfall perturbations have yet to be quantified. It needs to be mentioned that the 2D wavelet spectrum analysis has shown no evidence for the westward-propagating intraseasonal signals proposed in Sultan and Janicot (2000), possibly because these signals are weak and/or can only be observed during a relatively short time period.

4. Summary and discussion

The purpose of this study is to understand the seasonal variations in surface rainfall patterns within the West African monsoon system by means of the 6-yr (1998–2003) high-quality TRMM products, a 4-yr (2000–2003) QuikSCAT surface wind data, and the NCEP–NCAR reanalysis wind data (1998–2003). Surface mean rainfall tends to be concentrated along two latitudinal

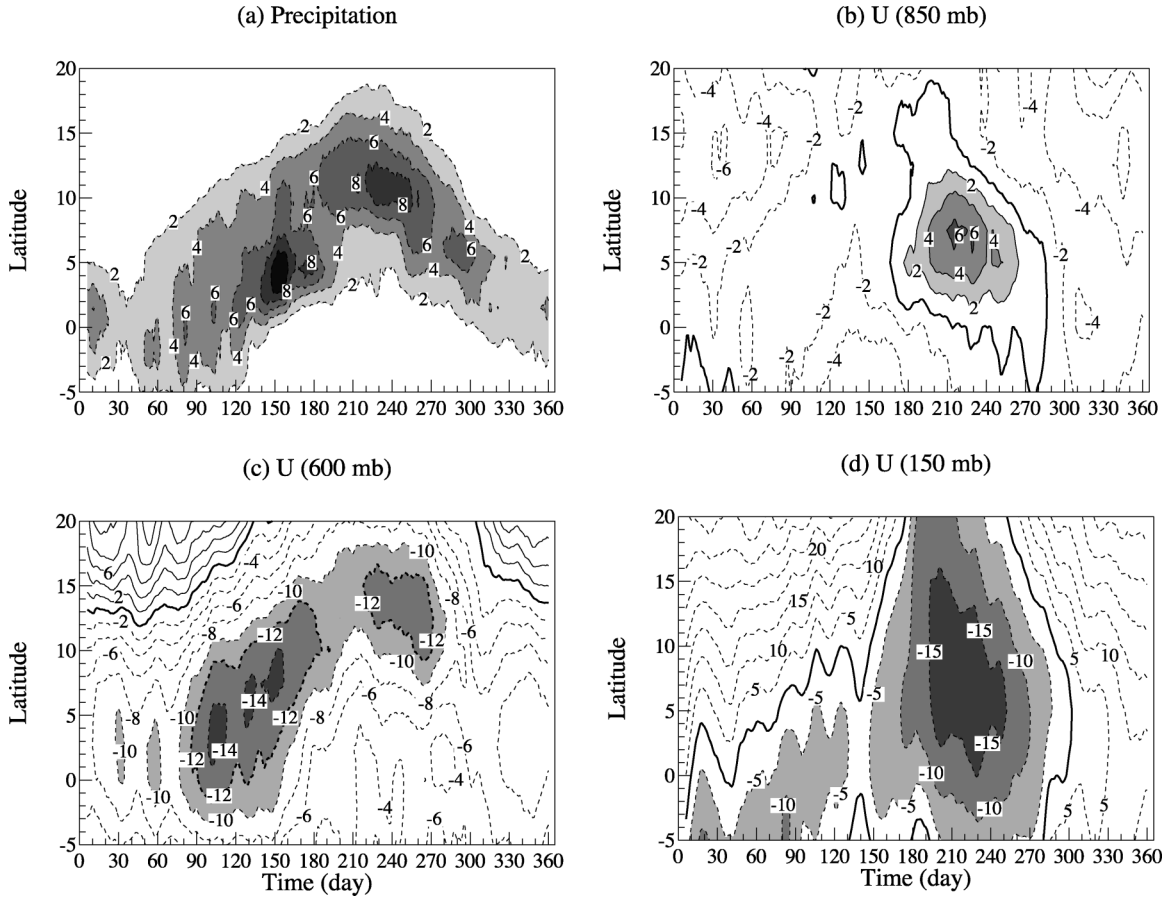

FIG. 6. Seasonal cycles in (a) daily rainfall (mm day^{-1}; 10-day running mean) from 3B42 between 9.5°W and 9.5°E, and daily *U* wind components (m s^{-1}; 10-day running mean) from the NCEP–NCAR Reanalysis Project at (b) 850 mb, (c) 600 mb, and (d) 150 mb between 10°W and 10°E.

belts: 5° and 10°N (Figs. 4a and 6a). The resulting two peak zones appear in two different seasons: April–June and July–September, respectively. In addition to the mean seasonal march, this pattern is manifested as a major rainfall zone ''jump'' over West Africa in the time–latitude diagrams as noted in past studies (e.g., Sultan and Janicot 2000; Le Barbe et al. 2002; Redelsperger et al. 2002). Surface rainfall and variability can generally be related to the large-scale processes. Furthermore, these two peak rainfall zones are actually associated with two different processes.

Near the Gulf of Guinea (about 5°N; Figs. 1–4), intense rainfall begins in April, apparently following the occurrence of warm SST in the tropical eastern Atlantic. Meridional SST gradients also play an essential role in forcing convection and rainfall during days 120–190 (approximately from May to mid-July; Fig. 4c), which is generally consistent with previous studies (e.g., Lindzen and Nigam 1987; Lau et al. 1997). Low-level southerly flow accelerates, possibly as a direct response to convection and rainfall, which induces the decrease in SST through an enhanced equatorial upwelling. Besides enhancing the southerly flow, the cold SST zone that forms quickly begins to suppress the convection and rainfall when the mean SST is less than about 27°C, although the strong meridional SST gradients still exist until about day 250 (Fig. 4c). The major deep convective zone is pushed northwestward along the coastline following the northward movement of warm water, rather than gradually moving northward across the land, probably due to the unfavorable surface conditions and the intrusion of dry air from the north (Sultan and Janicot 2003). Consequently the major surface rainfall events near the Gulf of Guinea disappear due to the formation of an oceanic cold tongue complex in the tropical eastern Atlantic. During this evolution, the surface rainfall is shown to be both a passive and active member in the entire coupled system. Other large-scale factors such as AEJ and TEJ, however, have not shown any significant impact in this region.

Along 10°N within the interior of West Africa (Figs. 4a and 6a), a second rain belt begins to develop in July and remains there during the later summer season. This belt seems to be independent of the first one to the south. The onset of rainfall events within this belt is concomitant with a northward movement of the AEJ and ac-

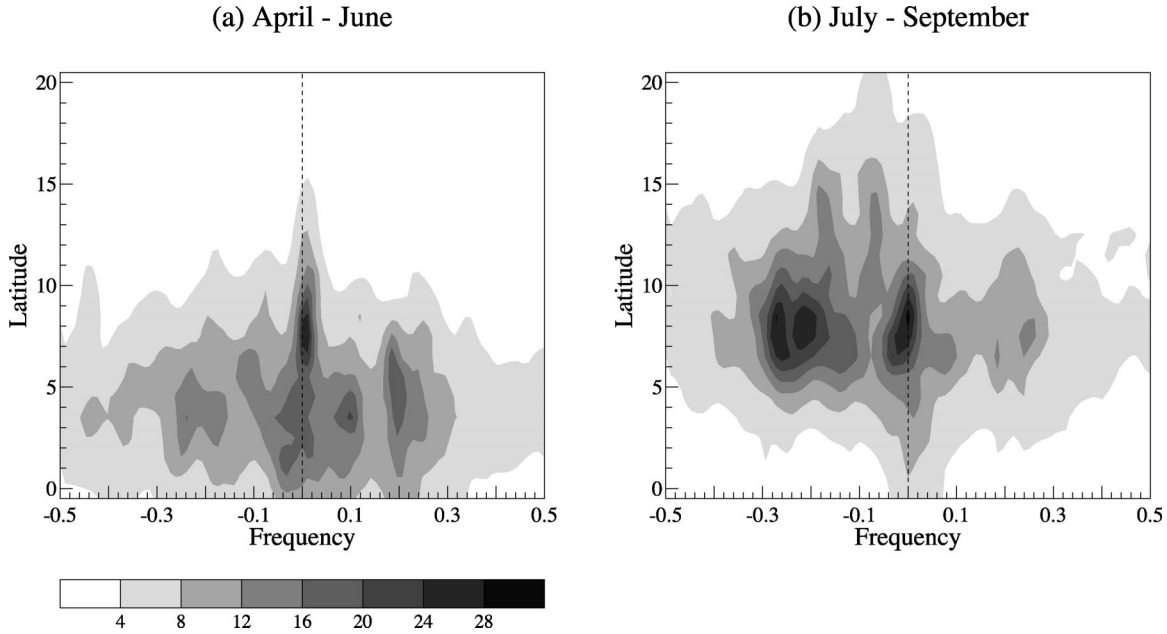

FIG. 7. Mean spectral power ($mm^2\ day^{-2}$; wavenumber $k = 6$ to 10) of rainfall from 3B42 between 9.5°W and 9.5°E during (a) Apr–Jun and (b) Jul–Sep as a function of frequency (cpd) and latitude. Positive (negative) frequencies represent eastward (westward) components.

companying horizontal and vertical shear zones (not shown), the appearance and strengthening of the TEJ and a strong low-level westerly flow, and the appearance of intense westward-propagating synoptic-scale wave signals (Figs. 6 and 7). Thus, rainfall and variability within the western African continent are primarily modulated by these large-scale features, such as the AEJ, TEJ, and low-level southwesterly flow, as suggested by previous studies (e.g., Grist and Nicholson 2001). However, the indirect dynamic effect of SST may not be negligible. Significant negative correlation between the SST in the tropical eastern Atlantic and the mean rainfall along 10°N is found (not shown) as in Opoku-Ankomah and Cordery (1994). Additionally, intense surface meridional SST gradients during days 190–250 are certainly favorable for the surface convergence zone and rainfall along 10°N (Fig. 4c).

There may also be a connection between the first rainfall peak and the AEJ (Fig. 6). Thorncroft and Blackburn (1999) indicated the importance of deep moist convection in the maintenance of the AEJ in a numerical simulation. A recent aircraft campaign further showed the modulations of mesoscale convective systems and associated convective heating on the AEJ (Thorncroft et al. 2003). The results in Fig. 6 tend to agree with them. Corresponding to the intense convection and rainfall during the boreal spring and early summer, the AEJ becomes very strong, right over or just north of the rainfall zone. The AEJ is directly connected to the appearance of the intense AEWs from July, which tend to weaken the intensity of the AEJ, possibly along with the major rain belt jump (actually a rainfall decrease) during the day 180–210 period (July). With the increase of surface rainfall along 10°N and/or a balance between the impacts of the AEWs and rainfall, the AEJ becomes stronger again during days 210–270. Thus, in addition to being an active member in the coupled system within the Gulf of Guinea, surface rainfall may also contribute to the evolution of the AEJ.

A 2D wavelet spectrum analysis provides a detailed decomposition of surface rainfall variability (Figs. 7 and 8). Most eastward-propagating (intraseasonal and synoptic-scale) wave signals are observed within the first peak rainfall zone during May–June. During July–September, in contrast, AEWs dominate the variability in the synoptic-scale domain within the second peak zone, even though eastward-propagating intraseasonal signals are still seen. This wave mode decomposition seems to enhance our argument on the seasonal variations of rainfall patterns over West Africa.

Tai and Ogura (1987) proposed that tropical easterly waves may be responsible for an abrupt 5° northward movement of the surface confluence line between June–July in the eastern Pacific. It seems that the AEWs can also be linked to the onset of rainfall events along 10°N due to their close relationships with the AEJ, TEJ, and low-level southwesterly flow. The appearance of the AEWs is concurrent with the weakening of the AEJ and the strengthening of the TEJ and low-level southwesterly flow. Hence, these waves may act as a major means for those large-scale features to modulate surface rainfall, especially the locations of rainfall events along 10°N, where the mean ITCZ is always located during the boreal summer. Certainly, we cannot exclude the

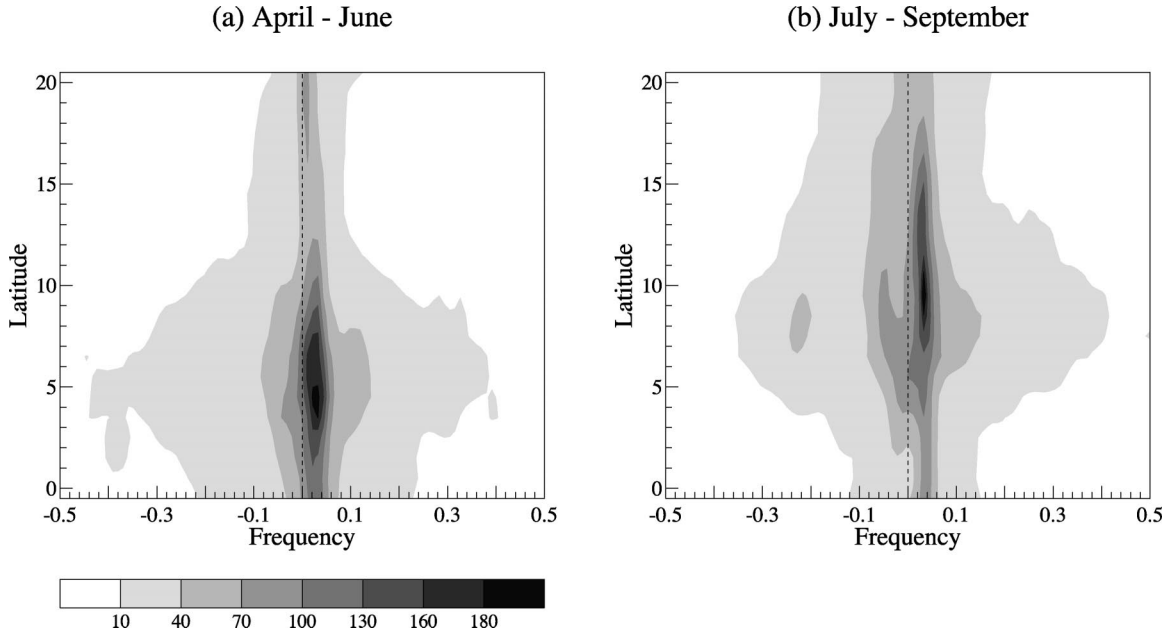

FIG. 8. Same as in Fig. 7, but for $k = 1$ to 5.

contributions from other mesoscale systems or random convective ones, although these systems may also be modulated or organized by the AEWs.

Consistent with Lebel et al. (2003), the West African continent may roughly be divided into two regions: south and north of about 6°–7°N. In these two regions, the seasonal cycles in surface rainfall are fundamentally different and are modulated by different processes, featuring two different peak rainfall seasons. This division may greatly enhance our understanding of seasonal rainfall distribution over West Africa and moreover further our knowledge of interannual and/or interdecadal variability in surface rainfall. However, it has to be pointed out that the conclusions made in this study are mostly based on direct observations. The actual cause–consequence relationships are much more complicated than we anticipated. Various feedbacks may always be active. Numerical models are required for further clarifications. These conclusions may also be tentative due to the lack of information on soil moisture, which may positively interact with rainfall (e.g., Nicholson 2000).

Finally, we mention that the relationship between surface rainfall and SST is evident here even on the weekly time scale, but the detailed mechanisms are far from clear. The 1-month lag between the peak SST and surface rainfall within the Gulf of Guinea clearly indicates the involvement of other factors such as meridional SST gradients and possibly large-scale motions (e.g., Lau et al. 1997). In addition, more quantitative examination is surely necessary.

Acknowledgments. The authors thank Prof. Chidong Zhang for commenting on an early version of the paper. We would also like to thank the editor, Dr. Hoerling, and two anonymous reviewers for their constructive comments and suggestions. Mr. David Bolvin prepared the TRMM 3B42 and 3B43 rainfall data. [Both TMI SST, water vapor, and cloud liquid water data and QuikSCAT sea surface wind (weekly and monthly) data were downloaded from http://www.ssmi.com.] NCAR–NCEP reanalysis data were provided by the NOAA–CIRES Climate Diagnostics Center, Boulder, Colorado, from its Web site (available online at http://www.cdc.noaa.gov). This work is supported through the Precipitation Missions Science Team under the NASA Headquarters TRMM Program Scientist Dr. Ramesh Kakar.

APPENDIX

Comparisons of Monthly Wind Products

Smith et al. (2001) found that the NCEP–NCAR reanalysis surface wind components are underestimated at all latitudes, compared with the World Ocean Circulation Experiment (WOCE) ship observations. Goswami and Sengupta (2003) confirmed this in the tropical Indian Ocean by means of the high-quality QuikSCAT wind fields. Since the NCEP–NCAR reanalysis wind products, especially the zonal wind component, are used to quantify the large-scale flow in this study, we seek to estimate the differences between them and QuiSCAT wind observations in the tropical Atlantic.

Seasonal cycles in the NCEP–NCAR 1000-mb wind components are calculated within a domain of 5°S–5°N, 10°W–5°E (dashed and dotted lines in Fig. 3c). The NCEP–NCAR 1000-mb zonal wind shows a seasonal cycle very similar to that of the QuikSCAT zonal wind, and their difference is approximately less than 1 m s^{-1}.

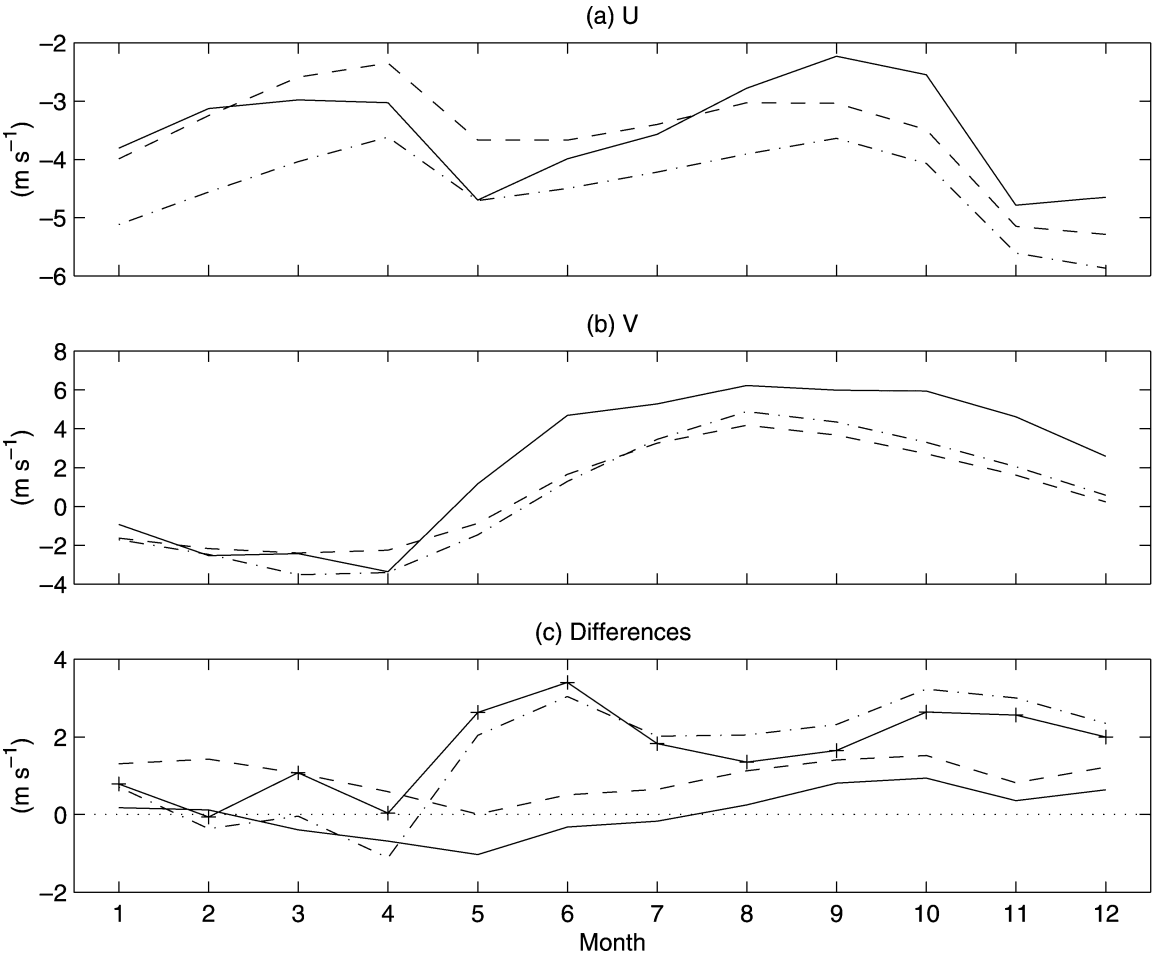

FIG. A1. (a), (b) Monthly mean QuikSCAT (m s^{-1}; solid lines), NCEP–NCAR reanalysis 1000-mb wind components (m s^{-1}; dashed lines), and NCEP–DOE AMIP-II reanalysis 1000-mb wind components (m s^{-1}; dashed–dotted lines) from 2000 to 2003. (c) The differences between QuikSCAT and NCEP–NCAR 1000-mb wind components (solid line for zonal wind, dashed–dotted line for meridional wind), and between QuikSCAT and NCEP–DOE AMIP-II reanalysis wind components (dashed line for zonal wind, crossed line for meridional wind). QuikSCAT wind components are averaged over 0.125°–5.125°N, 30.125°–20.125°W; the two reanalysis wind components are averaged over 0°–5°N, 30°–20°W.

However, large differences are found between the QuikSCAT and NCEP–NCAR 1000-mb meridional winds (dashed–dotted and dotted lines, respectively, in Fig. 3c), particularly during March–June, which actually results in two different seasonal cycles. Further comparisons are made within a domain in the tropical central Atlantic; 0.125°–5.125°N, 30.125°–20.125°W for QuikSCAT winds and 0°–5°N, 30°–20°W for the NCEP–NCAR 1000-mb winds (Fig. A1), where different seasonal evolution patterns in surface wind fields are found (not shown). The NCEP–NCAR 1000-mb zonal wind seems to be overestimated during March–July but underestimated primarily during September–December, which is a little different from Smith et al. (2001) and Goswami and Sengupta (2003). However, both zonal wind components show a very similar seasonal cycle, and their difference is less than 1 m s^{-1} as in Fig. 3c. For meridional winds, large differences are found during May–December. The NCEP–NCAR 1000-mb meridional wind is underestimated about 2–3 m s^{-1}, even though it has a similar seasonal cycle as the QuikSCAT meridional component. Compared with the NCEP–NCAR reanalysis, the NCEP–Department of Energy (DOE) Atmospheric Model Intercomparison Project (AMIP-II) reanalysis does not show much improvement (Fig. A1). Thus, both Figs. 3c and A1 provide confidence in both the NCEP–NCAR and NCEP–DOE AMIP-II zonal wind components but raise doubts regarding the application of their meridional wind fields.

REFERENCES

Adler, R. F., G. J. Huffman, D. T. Bolvin, S. Curtis, and E. J. Nelkin, 2000: Tropical rainfall distributions determined using TRMM combined with other satellite and rain gauge information. *J. Appl. Meteor.*, **39,** 2007–2023.

——, C. Kummerow, D. Bolvin, S. Curtis, and C. Kidd, 2003: Status of TRMM monthly estimates of tropical precipitation. *Cloud Systems, Hurricanes, and the Tropical Rainfall Measuring Mis-*

sion (TRMM): A Tribute to Dr. Joanne Simpson, Meteor. Monogr., No. 51, Amer. Meteor. Soc., 223–234.

Burpee, R. W., 1972: The origin and structure of easterly waves in the lower troposphere of North Africa. *J. Atmos. Sci.,* **29,** 77–90.

——, 1974: Characteristics of the North African easterly waves during the summers of 1968 and 1969. *J. Atmos. Sci.,* **31,** 1556–1570.

Eltahir, E. A. B., and C. Gong, 1996: Dynamics of wet and dry years in West Africa. *J. Climate,* **9,** 1030–1042.

Fontaine, B., and S. Janicot, 1996: Sea surface temperature fields associated with West African rainfall anomaly types. *J. Climate,* **9,** 2935–2940.

Goswami, B. N., and D. Sengupta, 2003: A note on the deficiency of NCEP/NCAR reanalysis surface winds over the equatorial Indian Ocean. *J. Geophys. Res.,* **108,** 3142, doi:10.1029/2002JC001497.

Grist, J. P., and S. E. Nicholson, 2001: A study of the dynamic factors influencing the rainfall variability in the West African Sahel. *J. Climate,* **14,** 1337–1359.

Grodsky, S. A., and J. A. Carton, 2001: Coupled land/atmospheric interaction in the West African Monsoon. *Geophys. Res. Lett.,* **28,** 1503–1506.

Gu, G., and C. Zhang, 2001: A spectrum analysis of synoptic-scale disturbances in the ITCZ. *J. Climate,* **14,** 2725–2739.

Hastenrath, S., 1991: *Climate Dynamics of the Tropics.* Kluwer Academic, 488 pp.

Hendon, H. H., and M. L. Salby, 1994: The life cycle of the Madden–Julian oscillation. *J. Atmos. Sci.,* **51,** 2225–2237.

Janicot, S., A. Harzallah, B. Fontaine, and V. Moron, 1998: West African monsoon dynamics and eastern equatorial Atlantic and Pacific SST anomalies (1970–88). *J. Climate,* **11,** 1874–1882.

Kalnay, E., and Coauthors, 1996: The NCEP/NCAR 40-Year Reanalysis Project. *Bull. Amer. Meteor. Soc.,* **77,** 437–471.

Laing, A. G., and J. M. Fritsch, 1993: Mesoscale convective complexes in Africa. *Mon. Wea. Rev.,* **121,** 2254–2263.

Lamb, P. J., and R. A. Peppler, 1992: Further case studies of tropical Atlantic surface atmospheric and oceanic patterns associated with sub-Saharan drought. *J. Climate,* **5,** 476–488.

Lau, K.-M., H.-T. Wu, and S. Bony, 1997: The role of large-scale atmospheric circulation in the relationship between tropical convection and sea surface temperature. *J. Climate,* **10,** 381–392.

Le Barbe, L., T. Lebel, and D. Tapsoba, 2002: Rainfall variability in West Africa during the years 1950–90. *J. Climate,* **15,** 187–202.

Lebel, T., A. Diedhiou, and H. Laurent, 2003: Seasonal cycle and interannual variability of the Sahelian rainfall at hydrological scales. *J. Geophys. Res.,* **108,** 8389, doi:10.1029/2001JD001580.

Li, T., and S. G. H. Philander, 1997: On the seasonal cycle of the equatorial Atlantic ocean. *J. Climate,* **10,** 813–817.

Lindzen, R. S., and S. Nigam, 1987: On the role of sea surface temperature gradients in forcing low-level winds and convergence in the Tropics. *J. Atmos. Sci.,* **44,** 2418–2436.

Liu, W. T., 2002: Progress in scatterometer application. *J. Oceanogr.,* **58,** 121–136.

——, W. Tang, and P. S. Polito, 1998: NASA Scatterometer provides global ocean-surface wind fields with more structures than numerical weather prediction. *Geophys. Res. Lett.,* **25,** 761–764.

Maloney, E. D., and J. T. Kiehl, 2002: MJO-related SST variability over the tropical eastern Pacific during Northern Hemisphere summer. *J. Climate,* **15,** 675–689.

Matthews, A. J., 2004: Intraseasonal variability over tropical Africa during northern summer. *J. Climate,* **17,** 2427–2440.

Merle, J., 1980: Seasonal heat budget in the equatorial Atlantic Ocean. *J. Phys. Oceanogr.,* **10,** 464–469.

Mitchell, T. P., and J. M. Wallace, 1992: The annual cycle in equatorial convection and sea surface temperature. *J. Climate,* **5,** 1140–1156.

Neelin, J. D., and I. M. Held, 1987: Modeling tropical convergence based on the moist static energy budget. *Mon. Wea. Rev.,* **115,** 3–12.

Nicholson, S. E., 2000: Land surface processes and Sahel climate. *Rev. Geophys.,* **38,** 117–139.

——, and J. P. Grist, 2003: The seasonal evolution of the atmospheric circulation over West Africa and equatorial Africa. *J. Climate,* **16,** 1013–1030.

——, and Coauthors, 2003: Validation of TRMM and other rainfall estimates with a high-density gauge dataset for West Africa. Part II: Validation of TRMM rainfall products. *J. Appl. Meteor.,* **42,** 1355–1368.

Opoku-Ankomah, Y., and I. Cordery, 1994: Atlantic sea surface temperatures and rainfall variability in Ghana. *J. Climate,* **7,** 551–558.

Redelsperger, J.-L., A. Diongue, A. Diedhiou, J.-P. Ceron, M. Diop, J.-F. Gueremy, and J.-P. Lafore, 2002: Multi-scale description of a Sahelian synoptic weather system representative of the West African Monsoon. *Quart. J. Roy. Meteor. Soc.,* **128,** 1229–1257.

Reynolds, R. W., and T. M. Smith, 1994: Improved global sea surface temperature analyses using optimum interpolation. *J. Climate,* **7,** 929–948.

Rowell, D. P., and J. R. Milford, 1993: On the generation of African squall lines. *J. Climate,* **6,** 1181–1193.

Smith, S. R., D. M. Lehler, and K. V. Verzone, 2001: Quantifying uncertainties in NCEP reanalyses using high-quality research vessel observations. *J. Climate,* **14,** 4062–4072.

Sultan, B., and S. Janicot, 2000: Abrupt shift of the ITCZ over West Africa and intra-seasonal variability. *Geophys. Res. Lett.,* **27,** 3353–3356.

——, and ——, 2003: The West African monsoon dynamics. Part II: The ''preonset'' and ''onset'' of the summer monsoon. *J. Climate,* **16,** 3407–3427.

——, ——, and A. Diedhiou, 2003: The West African monsoon dynamics. Part I: Documentation of intraseasonal variability. *J. Climate,* **16,** 3389–3406.

Tai, K.-S., and Y. Ogura, 1987: An observational study of easterly waves over the eastern Pacific in the northern summer using FGGE data. *J. Atmos. Sci.,* **44,** 339–361.

Thorncroft, C. D., and M. Blackburn, 1999: Maintenance of the African easterly jet. *Quart. J. Roy. Meteor. Soc.,* **125,** 763–786.

——, and Coauthors, 2003: The JET2000 project: Aircraft observations of the African easterly jet and African easterly waves. *Bull. Amer. Meteor. Soc.,* **84,** 337–351.

Weingartner, T. J., and R. H. Weisberg, 1991: A description of the annual cycle in sea surface temperature and upper ocean heat in the equatorial Atlantic. *J. Phys. Oceanogr.,* **21,** 83–96.

Wentz, F. J., 1997: A well-calibrated ocean algorithm for special sensor microwave/imager. *J. Geophys. Res.,* **102,** 8703–8718.

——, C. Gentemann, D. Smith, and D. Chelton, 2000: Satellite measurements of sea surface temperature through clouds. *Science,* **288,** 847–850.

Wheeler, M., and G. N. Kiladis, 1999: Convectively coupled equatorial waves: Analysis of clouds and temperature in the wavenumber–frequency domain. *J. Atmos. Sci.,* **56,** 374–399.

Zhang, C., 1993: Large-scale variability of atmospheric deep convection in relation to sea surface temperature in the Tropics. *J. Climate,* **6,** 1898–1912.